

Modeling the Dynamics of Heterogeneity of Solid Tumors in Response to Chemotherapy

Heyrim Cho¹ · Doron Levy² 

Received: 17 February 2017 / Accepted: 29 September 2017 / Published online: 11 October 2017
© Society for Mathematical Biology 2017

Abstract In this paper, we extend the model of the dynamics of drug resistance in a solid tumor that was introduced by Lorz et al. (Bull Math Biol 77:1–22, 2015). Similarly to the original, radially symmetric model, the quantities we follow depend on a phenotype variable that corresponds to the level of drug resistance. The original model is modified in three ways: (i) We consider a more general growth term that takes into account the sensitivity of resistance level to high drug dosage. (ii) We add a diffusion term in space for the cancer cells and adjust all diffusion terms (for the nutrients and for the drugs) so that the permeability of the resource and drug is limited by the cell concentration. (iii) We add a mutation term with a mutation kernel that corresponds to mutations that occur regularly or rarely. We study the dynamics of the emerging resistance of the cancer cells under continuous infusion and on–off infusion of cytotoxic and cytostatic drugs. While the original Lorz model has an asymptotic profile in which the cancer cells are either fully resistant or fully sensitive, our model allows the emergence of partial resistance levels. We show that increased drug concentrations are correlated with delayed relapse. However, when the cancer relapses, more resistant traits are selected. We further show that an on–off drug infusion also selects for more resistant traits when compared with a continuous drug infusion of identical total drug concentrations. Under certain conditions, our model predicts

✉ Doron Levy
dlevy@math.umd.edu

Heyrim Cho
hcho1237@math.umd.edu

¹ Department of Mathematics, University of Maryland, College Park, MD 20742, USA

² Department of Mathematics and Center for Scientific Computation and Mathematical Modeling (CSCAMM), University of Maryland, College Park, MD 20742, USA

the emergence of a heterogeneous tumor in which cancer cells of different resistance levels coexist in different areas in space.

Keywords Multi-drug resistance · Cancer dynamics · Diffusion

1 Introduction

Resistance to chemotherapy is a key obstacle to successful cancer treatments. Thus, the biological mechanisms responsible for the emergence of drug resistance and its propagation have been extensively studied (Gillet and Gottesman 2010; Teicher 2006). Those mechanisms involve genetic and/or epigenetic alternations that allow cancer cells to evade one or more drugs (Gottesman 2002; Gottesman et al. 2002; Fodal et al. 2011). In addition, the local tumor environment, including the availability of resources and reduced absorption or metabolism of drugs, provides ecological opportunities for resistant cells to evolve (Gerlinger et al. 2012; Rainey and Travisano 1998; Panetta 1998). The complexity of the underlying mechanisms has encouraged the development of mathematical models for describing the emergence and evolution of drug resistance. Such models were used for improving early detection, quantifying intrinsic and acquired resistance cells, and designing therapeutic protocols (Lavi et al. 2012; Michor et al. 2006; Foo and Michor 2014; Roose et al. 2007; Swierniak et al. 2009).

Mathematical approaches for modeling the growth of tumor and resistant cells range from deterministic to stochastic and from discrete (agent based) to continuum models (differential equations). Modeling the emergence of resistance was initiated in a series of work by Goldie and Coldman (1979, 1983a, b). These works predominantly concentrated on point mutations that lead to resistance. Their approach was extended using stochastic models including branching process and multiple mutations to study multi-drug resistance and optimal control of drug scheduling (Komarova 2006; Michor et al. 2006; Kimmel et al. 1998; Iwasa et al. 2006). Continuum deterministic models using ordinary differential equations were used as a complementary approach to study, for example, kinetic resistance (Birkhead et al. 1987) and point mutations (Tomasetti and Levy 2010). Spatial heterogeneity and vascularization were incorporated into models using partial differential equations (Anderson and Chaplain 1998; Trédan et al. 2007; Wu et al. 2013), integro-differential equations (Lorz et al. 2013; Greene et al. 2014).

Recent studies emphasize the importance of the tumor microenvironment as a driving force for drug resistance (Gerlinger et al. 2012; Bruin et al. 2013). Modeling the spatial dependency becomes more significant due to limited perfusion capability of large molecules and the differences in drug exposure based on their distance from the capillary bed (Minchinton and Tannock 2006; Trédan et al. 2007; Vaupel et al. 1989). Once spatially heterogeneous populations appear, they can also modulate the absorption and metabolism of the resources and drugs, which further promotes heterogeneity. Thus, various spatiotemporal models have been developed aiming at understanding the tumor morphology and phenotypic evolution driven by selective pressure from the microenvironment (Anderson et al. 2006; Trédan et al. 2007; Wu et al. 2013; Panagiotopoulou et al. 2010).

The present work is an extension of [Lorz et al. \(2013, 2015\)](#). The 2013 paper introduced a mathematical model for studying the effects of cytotoxic and cytostatic drugs on cancer cells. These two types of drugs have distinct effects on cancer cells. While cytotoxic drugs aim to destroy cancer cells, for instance, by damaging the DNA or inhibiting mitosis that lead to cell death, cytostatic drugs, i.e., antiproliferative drugs, suppress cell growth by arresting the cell cycle. However, exposures to these drugs may result in the development of numerous cell intrinsic and extrinsic drug resistance mechanisms, such as alterations to the target of drug, activation of a compensating pathway, environmental blockade, or alterations in drug metabolism. Thus, assuming a continuous trait variable that corresponds to the resistance level, Lorz et al. derived the long-term temporal dynamics of the fittest traits in the regime of small mutations. The model of [Lorz et al. \(2013\)](#) was extended in [Lavi et al. \(2013, 2014\)](#); [Greene et al. \(2014\)](#) by considering sufficiently large mutations and including cellular density effects. An extension to a radially symmetric spatial model was done in [Lorz et al. \(2015\)](#). Their work models the selection dynamics of cells taking into account the availability of resources and the diffusion of cytotoxic and cytostatic drugs.

Building on the model of [Lorz et al. \(2015\)](#), we develop in this paper a mathematical model that describes the dynamics of drug resistance in a solid tumor involving spatial diffusion and phenotypic mutation. The fundamental differences between our model and the original model are that we consider a growth rate function that allows for the emergence of partial resistance levels. This is unlike the original model for which the resistance levels asymptotically approached one of the boundaries: Over time, cancer cells ended up being either fully resistant or fully sensitive. Additional changes we make in the drug response function allow to model the effect of drug concentration in modulating the resistance level. Other two major modifications in the cell dynamics equation include a space diffusion and a mutation term. The new diffusion term incorporates cell motility into the model. No such effect was included in the original model. In addition, we adjust all diffusion terms in our system to depend on the cell density, so that the cell motility and the permeability of the resources and drugs are leveraged by the local cell concentration. Finally, our model involves a mutation term. We study the impact of different mutation kernels on the emerging drug resistance dynamics.

This paper is organized as follows. In Sect. 2, we review the model and the biological assumptions introduced in [Lorz et al. \(2015\)](#), which then leads us to introducing our model. Section 3 is divided into three subsections in which we study the three main modifications made with respect to the original model: the growth term, the diffusion term, and the mutation term. We demonstrate that our model provides an asymptotic trait distribution that is not necessarily concentrated on the boundaries of the domain. This stands in contrast to the model of [Lorz et al. \(2015\)](#) in which the cancer cells end up as a delta function being either fully resistant or fully sensitive. Since in our case the distribution is not necessarily attracted to the boundary of the trait variable, we can study how the various parameters impact the emerging dynamics of the drug resistance. Specifically, we demonstrate that an increased drug concentration results with a delayed relapse of the cells. However, once a relapse occurs, a higher drug dosage selects for more resistant cells. This also implies that an on-off drug schedule selects for more resistant cells than the cells that are selected by a corresponding continuous drug schedule (with the same total drug concentration). Finally, we demonstrate that

when combining spatial diffusion with mutations, a tumor may become spatially heterogeneous by developing regions in which different levels of resistance are expressed. Conclusions and future directions are discussed in Sect. 4.

2 Model and Assumptions

We start with a brief overview of the model in [Lorz et al. \(2015\)](#). This model describes the dynamics of the population density of the tumor cells $n(t, r, \theta)$. The model assumes a 2D radially symmetric setup with a normalized planar distance of cells from the center, given by $r \in [0, 1]$. The variable $\theta \in [0, 1]$ describes the normalized expression level of a cytotoxic-resistant phenotype, i.e., the level of resistance to cytotoxic agents. This can be related to a gene expression in a cellular level of cytotoxic drug resistance and proliferative potential, such as ALDH1, CD44, CD117, or MDR1 ([Amir et al. 2013](#); [Hanahan and Weinberg 2011](#); [Medema 2013](#)). In addition to the density of tumor cells, the model follows the dynamics of nutrients, $s(t, r) \geq 0$, a cytotoxic drug, $c_1(t, r) \geq 0$ and a cytostatic drug, $c_2(t, r) \geq 0$. The model is written as

$$\partial_t n(t, r, \theta) = [R(t, r, \theta) - D(\rho(t, r)) - \mu_1(\theta)c_1(t, r)]n(t, r, \theta) \tag{1}$$

$$- \alpha_s \Delta s(t, r) + \left[\gamma_s + \int_0^1 p(\theta)n(t, r, \theta)d\theta \right] s(t, r) = 0, \tag{2}$$

$$- \alpha_{c_1} \Delta c_1(t, r) + \left[\gamma_{c_1} + \int_0^1 \mu_1(\theta)n(t, r, \theta)d\theta \right] c_1(t, r) = 0, \tag{3}$$

$$- \alpha_{c_2} \Delta c_2(t, r) + \left[\gamma_{c_2} + \mu_2 \int_0^1 n(t, r, \theta)d\theta \right] c_2(t, r) = 0. \tag{4}$$

The first term on the RHS of Eq. (2) is a growth term,

$$R(t, r, \theta) = R(t, r, \theta; s, c_2) = \frac{p(\theta)}{1 + \mu_2 c_2(t, r)} s(t, r).$$

Here, $p(\theta) > 0$ models the consumption of the resource depending on the resistance level. In Sect. 3, we will demonstrate that the choice of an appropriate consumption function $p(\theta)$ plays a key role in controlling the emerging dynamics. It is assumed that cells that are resistant to cytotoxic drugs use their resources to developing and maintaining the drug resistance mechanism ([Mumenthaler et al. 2015](#); [Wosikowski et al. 2000](#)), corresponding to $p'(\theta) < 0$. The cytostatic drug $c_2(t, r)$ reduces the proliferation rate, with an uptake constant μ_2 .

The second term on the RHS of Eq. (2) is a death rate $D(\rho)$, which we assume is of the form $D(\rho) = d\rho(t, r)$. It is proportional to the local number of cells $\rho(t, r)$

$$\rho(t, r) = \int n(t, r, \theta)d\theta, \tag{5}$$

with a constant death rate d . The third term on the RHS of Eq. (2) represents the death of cancer cells due to the action of the cytotoxic drug $c_1(t, r)$, where $\mu_1(\theta)$ is the drug

uptake function. We assume that as the resistance level increases, the cells become more resilient to cytotoxic drugs, that is, $\mu'_1(\theta) < 0$.

In Eqs. (3)–(4), Δ denotes the Laplacian operator describing the diffusion in the radial direction, the α 's are the diffusion constants, and the γ 's provide a decay of the corresponding terms.

The system is augmented with zero Neumann boundary conditions at $r = 0$, and a source term at $r = 1$, written as Dirichlet boundary conditions

$$\begin{aligned} \partial_r s(t, r = 0) &= 0, & s(t, r = 1) &= S_1, \\ \partial_r c_i(t, r = 0) &= 0, & c_i(t, r = 1) &= C_i(t), \quad i = 1, 2. \end{aligned} \tag{6}$$

The models (2)–(4) provide a framework for studying the emergence of drug resistance, incorporating the resource and the two types of drugs. However, while the spatial heterogeneity is determined by the local environment, the heterogeneity in the phenotypic space is driven by the growth term including the resource consumption $p(\theta)$ and cytotoxic drug uptake $\mu_1(\theta)$. Thus, the dependency of these factors on the phenotypic variable can be further studied. In addition, at each spatial location, the cancer cell equation is only governed by an exponential growth term that lacks the effect of spatial diffusivity and resistance driven by mutation. As will be demonstrated in Sect. 3, the models (2)–(4) asymptotically converge to a distribution of cells that are concentrated on the boundary of the interval, either fully resistant or fully sensitive cells.

To address these issues, we replace the model (2)–(4) by the following system

$$\begin{aligned} \partial_t n(t, r, \theta) &= [((1 - w)R(t, r, \theta) - D(\rho(t, r)) - C(t, r, \theta))]n(t, r, \theta) \\ &\quad + \alpha_n(\rho(t, r))\Delta n(t, r, \theta) + w \int R(t, r, \vartheta)M(\theta, \vartheta)n(t, r, \vartheta)d\vartheta, \end{aligned} \tag{7}$$

$$-\alpha_s(\rho(t, r))\Delta s(t, r) + \left[\gamma_s + \int_0^1 p(\theta)n(t, r, \theta)d\theta \right] s(t, r) = 0, \tag{8}$$

$$-\alpha_{c_1}(\rho(t, r))\Delta c_1(t, r) + \left[\gamma_{c_1} + \int_0^1 \mu_1(\theta)n(t, r, \theta)d\theta \right] c_1(t, r) = 0, \tag{9}$$

$$-\alpha_{c_2}(\rho(t, r))\Delta c_2(t, r) + \left[\gamma_{c_2} + \mu_2 \int_0^1 n(t, r, \theta)d\theta \right] c_2(t, r) = 0. \tag{10}$$

Equation (7) involves three terms: a reaction term describing the growth rate, a spatial diffusion term, and a mutation term represented by an integral operator. The growth term consists of a natural growth rate $R(t, r, \theta)$, a natural death term $D(\rho)$, and a death term due to the cytotoxic drug $C(t, r, \theta)$. Both R and D are assumed to be of the same form as in Eq. (2). The effect of the cytotoxic drug is modeled as $C(t, r, \theta; c_1) = \mu_1(\theta, c_1)c_1(t, r)$, where $\mu_1(\cdot, \cdot) > 0$ is an uptake function that not only depends on θ , but also depends on the cytotoxic drug c_1 . Similar to Eq. (2), we assume that $\partial_\theta \mu_1(\cdot, c_1) < 0$ as to model the resilience of the resistance cells, but also, $\partial_{c_1} \mu_1(\cdot, c_1) < 0$ for drug-induced resistance. This is motivated from the experiments in Mumenthaler et al. (2015) where the net growth rate of a certain type of resistant

Table 1 List of variables and functions

Variable/function	Range	Biological interpretation
r	$[0, 1]$	Radial spatial variable
θ	$[0, 1]$	Resistance level
t	\mathbb{R}_+	Time
$n(t, r, \theta)$	\mathbb{R}_+	Concentration of cells with phenotype θ at (t, r)
$s(t, r)$	\mathbb{R}_+	Density of resources
$c_1(t, r)$	\mathbb{R}_+	Density of cytotoxic drugs
$c_2(t, r)$	\mathbb{R}_+	Density of cytostatic drugs
$\rho(t, r)$	\mathbb{R}_+	Total number of cells at (t, r)
d	\mathbb{R}_+	Death rate
$\mu_1(\theta, c_1), \mu_2$	\mathbb{R}_+	Drug uptake rate
$M(\theta, \vartheta)$	$[0, 1]$	Probability of mutation from phenotype ϑ to θ
w	$[0, 1]$	Proportion of cells undergoing mutation
$\alpha_n, \alpha_s, \alpha_{c_1}, \alpha_{c_2}$	\mathbb{R}_+	Cell motility and permeability
$\gamma_s, \gamma_{c_1}, \gamma_{c_2}$	\mathbb{R}_+	Decay coefficient

cells is distinctive in different levels of drug concentration. As will be demonstrated later, it is important to consider an uptake function $\mu_1(\theta, c_1)$ that also depends on the cytotoxic drug c_1 . This allows us to more realistically model the dynamics of the effectiveness of the cytotoxic drug.

We consider a spatial diffusion in the cancer cell density equation with a coefficient α_n in order to model the cell motility. We assume a zero Neumann boundary condition at both boundaries for the cells concentration,

$$\partial_r n(t, r = 0) = \partial_r n(t, r = 1) = 0.$$

The diffusion in the resource, cytotoxic drug, and cytostatic drug is known to play an important role in spatial heterogeneity (Lorz et al. 2015). In addition, the tumor pressure is identified as one of the critical features that affect the efficacy of cancer treatment (Ariffin et al. 2014). Unlike the original model where the diffusion coefficients α_s, α_{c_1} , and α_{c_2} were assumed to be constants, we assume that the diffusion coefficients are functions of the number of cells $\rho(t, r)$. Our model allows to consider the influence of density of the tumor on the motility and permeability of the nutrients and the drugs.

The integral term in the cell density equation accounts for the mutation. The weight $0 \leq w \leq 1$ denotes the fraction of cells with phenotype θ that undergoes mutation and the remaining $1 - w$ undergo faithful division. More generally, the weight can be modeled as a function of the trait variable, i.e., $w = w(\theta)$. The Mutation kernel $M(\theta, \vartheta) \geq 0$ is the probability that phenotype ϑ will be mutated into phenotype θ . Thus, we assume conservation, $\int_0^1 M(\theta, \vartheta) d\vartheta = 1$ for $\forall \theta \in [0, 1]$. All model parameters including their ranges and biological interpretation are listed in Table 1.

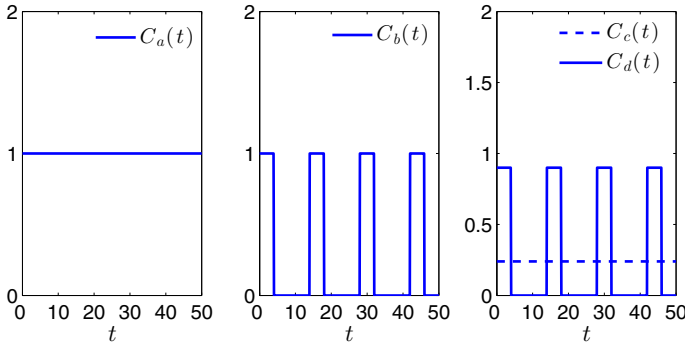


Fig. 1 Drug infusion schemes used in our simulations, either a constant infusion $C_a(t)$ and $C_c(t)$ or an on–off infusion $C_b(t)$ and $C_d(t)$

3 Model and Simulation

In this section, we study the role of each term in the models (7)–(10) in detail, namely the growth rate, the diffusion terms, and the mutation term. The numerical results are analyzed by comparing the phenotype distribution of the cancer cells and the total number of cells defined as

$$q(t, \theta) := \int_0^1 n(t, r, \theta)r^2 dr, \quad \rho_T(t) := \int_0^1 \int_0^1 n(\theta, r, t)r^2 dr d\theta,$$

respectively. In addition, we denote the normalized probability density function of the phenotype as $Q(t, \theta) := q(t, \theta)/\rho_T(t)$.

Following [Lorz et al. \(2015\)](#) the initial distribution of the cancer cells is taken as

$$n(t = 0, r, \theta) = C^0 \exp \left[\frac{-(\theta - 0.5)^2}{\varepsilon} \right]. \tag{11}$$

This mimics a biological scenario where most of the cells are characterized by the intermediate level of resistance $\theta = 0.5$ to therapies. We also take $C^0 = 0.005 \ll 1$ and $\varepsilon = 0.005 \ll 1$ assuming, following [Lorz et al. \(2015\)](#), that we are dealing with a tumor spheroid of small size where micro-tumors are derived from a single cell clone.

The resource is supplied in a constant level as $S_1 = 12$ that is imposed as the boundary condition in Eq. (6). For the drug infusion, we consider a combination of two types of dose schemes, either a continuous infusion $C_a(t)$ or an on–off infusion $C_b(t)$ as shown in Fig. 1. We denote the interval of the on–off scheme being nonzero on interval $I_{bb} = \cup_{n \in \mathbb{N}_0} [nT, nT + T_{bb}]$, that is, $C_c(t \notin I_{bb}) = 0$. Here, T is the period and T_{bb} is the time where the drug is infused. For a fair comparison between different drug schemes, the dosages are selected in such a way that the total dose delivered remains the same over a time interval $[0, T]$. For instance, $C_c(t) = 0.24C_a(t)$ and $C_d(t) = 0.84C_b(t)$ for $T = 14$ and $T_{bb} = 4$, so that $\int_0^T C_c(t)dt = \int_0^T C_d(t)dt$. Following [Lorz et al. \(2015\)](#) we choose three different dose schedules. The first two

include no cytostatic drug and either a constant or an on–off infusion for the cytotoxic drug $C_1(t)$, that is,

$$\text{Schedule 1: } C_1(t) = kC_a(t), \quad C_2 = 0,$$

$$\text{Schedule 2: } C_1(t) = kC_b(t), \quad C_2 = 0,$$

with some constant k . In addition, we consider a combination of the cytotoxic and cytostatic drug

$$\text{Schedule 3: } C_1(t) = C_d(t), \quad C_2(t) = C_c(t).$$

Schedule 3 is shown in [Lorz et al. \(2015\)](#) to be the best dose scheme for the model (2)–(4) when taking into account the cell growth and the resistance level.

3.1 Phenotype Selection Depending on Cytotoxic Drug

We start by investigating the growth rate in Eq. (7). This growth rate is based on three terms: the natural division rate $R(t, r, \theta)$, the death rate $D(\rho)$, and the response to the cytotoxic drug $C(t, r, \theta)$. Here, to focus on the role of these terms, we neglect the diffusion in $n(t, r, \theta)$ and the mutation terms by taking $\alpha_n = 0$ and $w = 0$.

First, we show that the long-time dynamics of the system in [Lorz et al. \(2015\)](#) can be categorized into few distinct scenarios as it has been proven in [Lorz et al. \(2013\)](#), and [Greene et al. \(2014\)](#). To simplify the analysis, we consider constant infusion of resources and cytotoxic drugs for the boundary condition in Eq. (6). We also assume that the death rate D is independent of the total cell density ρ . With an appropriate choice of numerical discretization, the semi-discretized system of Eq. (7) can be considered as a system of ordinary differential equations of the grid point values r_k of the solution, that is, $n_k = n(t, r_k, \theta)$. For instance, we can take a finite difference discretization or collocation basis functions at the grid points, such as Lagrangian polynomials. In addition to time-independent boundary conditions, we assume that Eqs. (9)–(10) have constant decay coefficients,^{1,2} then the system becomes

$$\partial_t n_k = \left(\hat{R}_k(\theta) - \hat{D}(\theta) - \hat{C}_k(\theta) \right) n_k, \tag{12}$$

and we can directly apply Theorem 1 in [Lorz et al. \(2013\)](#) and [Greene et al. \(2014\)](#). The theorem describes the two qualitatively distinct scenarios as follows:

Theorem 1 Consider Eq. (12) with initial condition $n_k(0, \theta)$. If $\hat{R}_k(\theta) < \hat{D}(\theta) + \hat{C}_k(\theta), \forall \theta \in [0, 1]$, then

$$\lim_{t \rightarrow \infty} n_k(t, \theta) = 0, \quad \forall \theta \in [0, 1], \quad \lim_{t \rightarrow \infty} \rho_k(t) = 0.$$

¹ Since the perturbations in the decay coefficients are small, for instance, $\gamma_s \gg \int_0^1 p(\theta)n(t, r, \theta)d\theta$, this estimation is similar to our simulation.

² The solutions can be explicitly written in terms of a modified Bessel function of the first kind $I_0(r)$ as $s(r) = S_1 I_0(\sqrt{\lambda_s}r) / I_0(\sqrt{\lambda_s})$, where $\lambda_s = \gamma_s/\alpha_s$, and similarly for $c_1(r)$ and $c_2(r)$. Then, $\hat{R}_k(\theta) = \frac{p(\theta)}{1+\mu_2 c_2(r_k)} s(r_k)$ and $\hat{C}_k(\theta) = \mu_1(\theta)c_1(r_k)$.

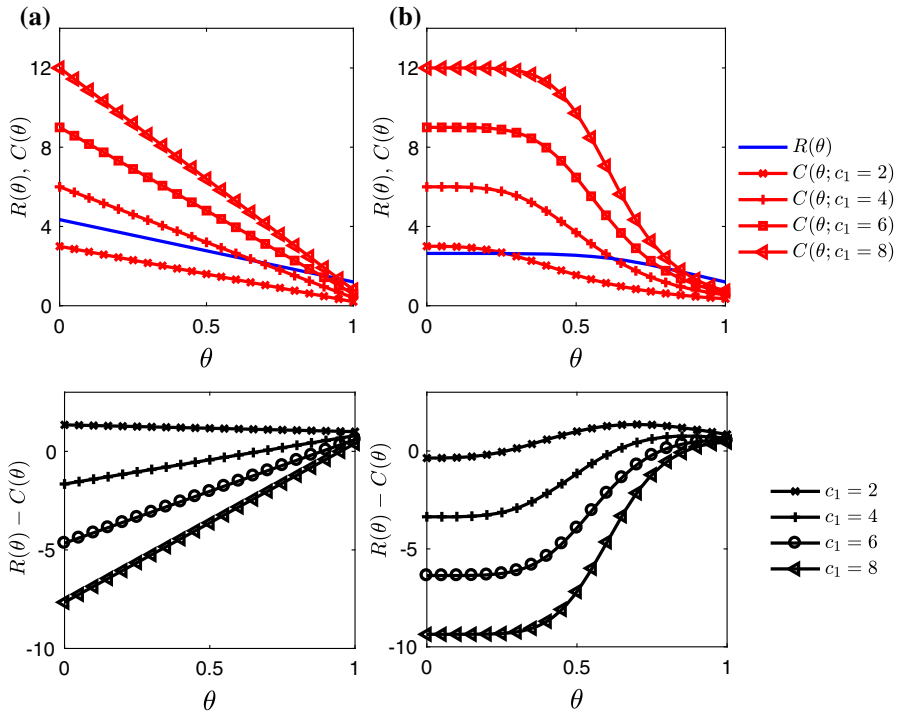


Fig. 2 Comparison of the growth term $R(t, r, \theta)$ and the drug effect $C(t, r, \theta)$. The second row plots the net growth rate $R(\theta) - C(\theta)$. **a** linear uptake and drug functions (Lorz et al. 2015). **b** nonlinear functions (13). In both figures, $s(t, r) = 12$ and $c_1(t, r) = c_1$

Alternatively, if there exists a $\theta \in [0, 1]$ such that $\hat{R}_k(\theta) > \hat{D}(\theta) + \hat{C}_k(\theta)$, then

$$\lim_{t \rightarrow \infty} \frac{n_k(\theta, t)}{\rho_k(t)} = \sum_{i=1}^m \mathbf{a}_i \delta(\theta - \theta_i),$$

where $\delta(\cdot)$ denotes the Dirac delta function, \mathbf{a}_i are positive constants such that $\sum_{i=1}^m \mathbf{a}_i = 1$, and

$$\theta_i = \arg \max_{0 \leq \theta \leq 1} \left(\hat{R}_k(\theta) - \hat{D}(\theta) - \hat{C}_k(\theta) \right).$$

The simplest form of the proliferation and drug uptake functions is linear (Grothey 2006; Brodie 1992), i.e., $p(\theta) = a_1\theta + a_2$ and $\mu(\theta) = b_1\theta + b_2$, respectively. As described in Sect. 2, both functions should have a negative derivative with respect to the phenotype θ , i.e., $a_1 < 0$ and $b_1 < 0$. Figure 2 (left) shows the growth term $R(t, r, \theta)$ and the drug effect $C(t, r, \theta)$ for the linear model with the coefficients prescribed as in Lorz et al. (2013). We note that the maximum growth rate without the cytotoxic drug, $R(\theta)$, is achieved at the boundary of the trait $\theta = 0$, which also corresponds to the case of only using cytostatic drugs. On the other hand, when a sufficiently large amount of

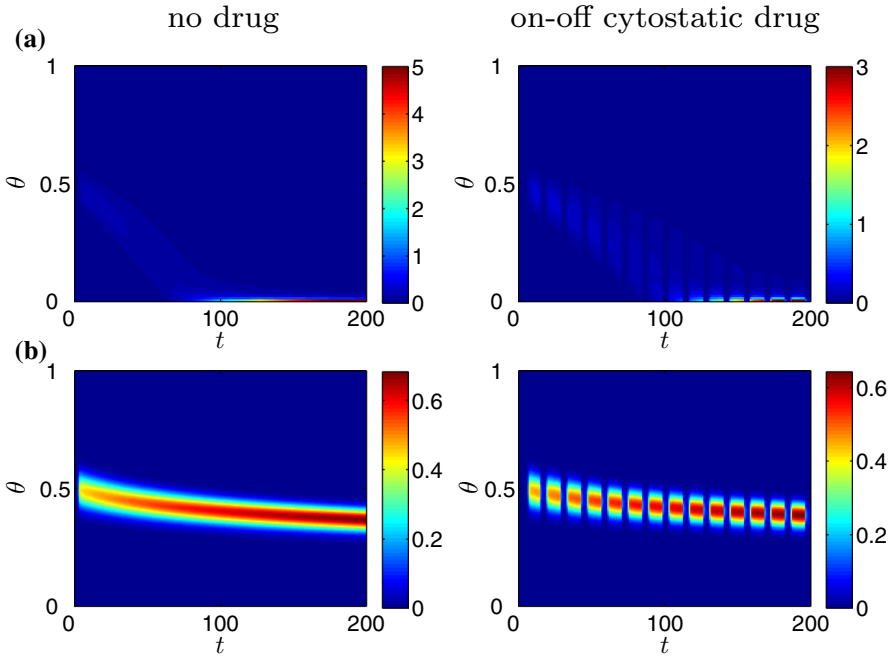


Fig. 3 The trait distribution of the cancer cells $q(t, \theta)$ for $t \in [0, 200]$. The shown results are computed with **a** the linear resource and uptake functions (Lorz et al. 2015); and **b** nonlinear functions. The left column is calculated with no drug, and the right column is calculated with an on–off infusion of the cytostatic drug. In the linear model, the trait distribution becomes a delta function at the (fully sensitive) boundary $\theta = 0$. The nonlinear model exhibits dynamics in which the limit distribution is heterogeneous and is not necessarily concentrated on the boundary

cytotoxic drug is applied, the growth rate $R(\theta) - C(\theta)$ is maximized at $\theta = 1$. Thus, by Theorem 1, the density function of the traits approaches a delta function that is concentrated at the boundary. For example, with a sufficient amount of cytotoxic drug using schedule 1 or 2, the density function of the traits approaches a delta function located at $\theta = 1$, while for cytostatic drug or no drug, the density function of the traits approaches a delta function at $\theta = 0$. This corresponds to the first row of Figs. 3 and 4.

To overcome an asymptotic solution in the form of a delta function at $\theta = 0$ or $\theta = 1$, we propose to replace the linear proliferation and drug uptake functions by nonlinear functions, inspired by Greene et al. (2014). We assume functions of the form:

$$p(\theta) = \frac{a_1}{1 + a_2\theta^5}, \quad \mu_1(\theta, c_1) = \frac{b_1}{1 + b_2\theta b_3}. \tag{13}$$

Here, a_1, a_2, b_1 are positive constants, and $b_2 := b_2(c_1), b_3 := b_3(c_1)$ are positive functions. Since $\partial_\theta p(0) \ll 1$ and $\partial_\theta \mu_1(0) \ll 1$, this choice avoids a blowup at $\theta = 0$. The parameters chosen for the simulations are estimated as follows: First, we assume the Norton–Simon hypothesis (Simon and Norton 2006) in which the rate of regression under chemotherapy is related to the rate of tumor growth:

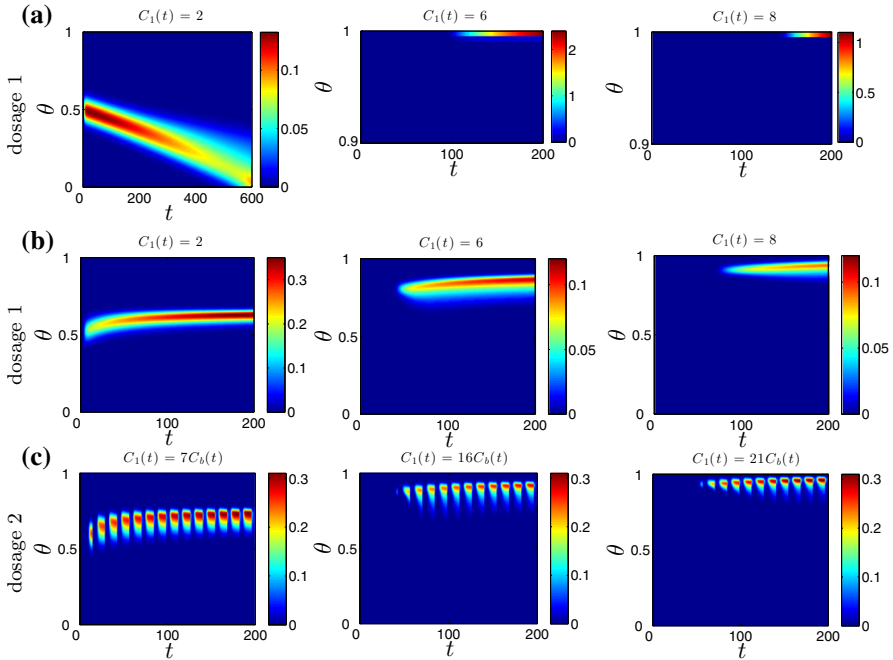


Fig. 4 The trait distribution of cancer cells $q(t, \theta)$. **a** linear resource and uptake functions (Lorz et al. 2015). **b, c** nonlinear resource and uptake functions Eq. (13). Figures **a** and **b** correspond to schedule 1, while figure **c** corresponds to schedule 2. The columns (from left to right) represent increased dosage. The figures for the linear model with dosage $C_1(t) = 4, 6$ are zoomed on $0.9 \leq \theta \leq 1$ to emphasize the asymptotic concentration of the density at $\theta = 1$. In the nonlinear model, a higher dosage of the cytotoxic drug results with a delayed relapse with higher resistance levels **a** dosage 1 **b** dosage 1 **c** dosage 2

$$\frac{a_1}{1 + a_2} \propto \frac{b_1}{1 + b_2}. \tag{14}$$

We further set the average proliferation rate and the average mortality rate due to the effect of cytotoxic drugs to the following constants (Corbett et al. 1975; Grothey 2006).

$$\int_0^1 p(\theta)d\theta \approx 0.2, \quad \int_0^1 \mu_1(\theta, c_1)d\theta \approx 0.8. \tag{15}$$

In particular, we choose $a_1 = 0.22, a_2 = 1.2$, and $b_1 = 1.5$, and the functions $b_2(c_1) = 5 + 1.25c_1$ and $b_3(c_1) = 2 + 0.5c_1$, see Pillis et al. (2005, 2014). The corresponding growth and drug effect functions are plotted in Fig. 2 for different values of c_1 . We observe that both functions are less steep near $\theta = 0$ and the maximal value of $R(t, r, \theta) - C(t, r, \theta)$ is achieved away from $\theta = 1$.

Figure 3 compares the growth of the cancer cells in the linear and nonlinear models for the cases without the cytotoxic drug. Shown is the cell concentration with respect to the traits $q(t, \theta)$ computed up to $t = 200$, without the drug and with the cytostatic drug. As expected from the theorem, without the cytotoxic drug, the trait distribution using

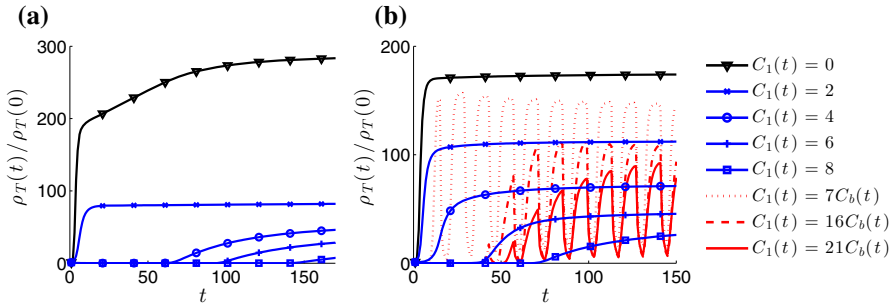


Fig. 5 The total number of cancer cells relative to the initial condition $\rho_T(t)/\rho_T(0)$. **a** the linear model, **b** the nonlinear model. The different drug schedules correspond to Figs. 3 and 4

the linear model becomes a delta function at $\theta = 0$. On the other hand, the nonlinear model (13) prevents the density function from blowing up at the boundary. Figure 4 shows the results of using the drug schedules for the cytotoxic drug. The linear model (shown in the first row) with sufficiently large dosage, for instance, $C_1(t) = 6, 8$, sends the trait distribution to a delta function at $\theta = 1$. We note that the figures are plotted in the range $0.9 \leq \theta \leq 1$ to visualize the concentration of density at $\theta = 1$. In our parameter setting, the threshold dosage is 2.25, and a dosage lower than the threshold asymptotically results with a distribution that approaches a delta function at $\theta = 0$. This is demonstrated for $C_1(t) = 2$ in Fig. 4 (upper left), where the computation is carried out until $t = 600$. In contrast to the linear case, the nonlinear model results in an asymptotic distribution centered around an intermediate resistance level $0 < \theta < 1$. The width of the asymptotic distribution shown in Fig. 4 is still rather narrow. We will later study factors that control this spread in heterogeneity.

As shown in Fig. 2, the maximum value of $R(t, r, \theta) - C(t, r, \theta)$ is achieved at a higher level of resistance trait as the cytotoxic drug dosage c_1 increases. In Fig. 4b, c we plot the cell concentration with respect to the traits $q(t, \theta)$ using continuous $C_a(t)$ and on-off $C_b(t)$ drug schemes for the cytotoxic drug $C_1(t)$. The corresponding total number of cells relative to the initial value is plotted in Fig. 5. We observe that a high dosage of cytotoxic drug delays the time of relapse. However, when a relapse occurs, cells with higher resistance level are selected. In particular, the delayed relapse in our simulations is consistent with the experiments in Mumenthaler et al. (2015) and Garvey et al. (2016), where the resistant cells have positive but less growth rates in higher drug dosages. In addition, the on-off scheme for the cytotoxic drug selects for more resistant cells than those selected by the corresponding continuous schedule with the same total dose. Temporarily, there is a reduction in the cancer cell population. Asymptotically, larger populations emerge with a higher resistance level. We note that considering different distributions in the initial density other than (11) affects the time of relapse, although the dominating resistance trait will be similar.

Finally, we comment that with an appropriate death rate function $D(\rho)$, the boundedness of the total number of cancer cell is provided by Theorem 2 in Greene et al. (2014). Based on the assumption of the theorem, the death rate function must satisfy $\lim_{\rho \rightarrow \infty} D(\rho) = \infty$. In particular, we choose $D(\rho) = \bar{d}\rho$, with a constant death rate

\bar{d} . Then, for the semi-discretized version of Eq. (7),

$$\partial_t n_k = \left(\hat{R}_k(\theta) - \bar{d}\hat{\rho}_k - \hat{C}_k(\theta) \right) n_k, \tag{16}$$

and the diffusion Eqs. (9), (10) with time-independent boundary conditions and decay coefficients, Theorem 2 in [Greene et al. \(2014\)](#) provides the following result,

Theorem 2 *In the semi-discretized system Eq. (16), with finite positive constants R_k^M and C_k^m ³, there exists $\exists \hat{\rho}_k^M < \infty$ such that*

$$0 < \hat{\rho}_k(t) \leq \hat{\rho}_k^M, \quad \forall t \geq 0,$$

and $\rho_T(t) \leq \max_k \hat{\rho}_k^M$

Our simulation results shown in Fig. 5 confirm the results of Theorem 2.

3.2 Phenotype Variability Depending on Spatial Diffusion

It is well known that the spatial component and the diffusion play a crucial role in heterogeneous cancer growth ([Lorz et al. 2015](#); [Anderson et al. 2006](#); [Trédan et al. 2007](#); [Wu et al. 2013](#); [Panagiotopoulou et al. 2010](#)). In this section, we study how the diffusion terms effect the cancer growth and the phenotypic heterogeneity in the resistance level. The diffusion terms in our system can be classified into two groups: (i) the cell motility modeled as a diffusion process with coefficient α_n in Eq. (7); and (ii) the permeability of the resource and the drugs with coefficients α_s, α_{c_1} , and α_{c_2} in Eqs. (9), (10). We aim to examine the role of these diffusion terms in our model. The coefficients are initially taken as constants, which allows us to study the sensitivity with respect to the magnitude of each term. We then model the coefficient as a function of $\rho(t, r)$ to further include the influence of cell density.

We first consider a constant infusion scheme of the cytotoxic drug $C_1(t) = 4C_a(t)$ and test for different values of permeability of the resource and the cytotoxic drug without cell mobility, i.e., setting $\alpha_n = 0$. We vary α_s and α_{c_1} by an order of magnitude from 0.08 to 0.8. In order to consider the same amount of the resource and drug across different permeabilities, we impose the boundary condition in Eq. (6) so that $\int_0^1 s(t = 0, r)r^2 dr$ is preserved. Here, $s(t = 0, r)$ is the solution to Eq. (9) with $n(t, r, \theta) = 0$ assuming that no cancer cells are present. The reference solution is taken as the case of $\alpha_s = 0.08$ and $S_1 = 12$. Then, the boundary condition for $\alpha_s = 0.25$ and $\alpha_s = 0.8$ becomes $S_1 = 9.08$ and $S_1 = 7.91$, respectively.

The cell concentration surface $n(t, r, \theta)$ at $t = 100$ and the phenotype distribution $q(t, \theta)$ up to time $t = 200$ for different values of α_s and α_{c_1} are plotted in Figs. 6

³ $R_k^M = \max_{\theta} \left[\frac{p(\theta)}{1+\mu_2 c_2(r_k)} s(r_k) \right]$, $C_k^m = \min_{\theta} [\mu_1(\theta)c_1(r_k)]$. Space independent bounds can be given as $R^M = \max_{\theta} \left[\frac{p(\theta)}{1+\mu_2 C_2/I_0(\sqrt{\lambda_{c_2}})} S_1 \right]$ and $C^m = \min_{\theta} [\mu_1(\theta)C_1/I_0(\sqrt{\lambda_{c_1}})]$, where $I_0(r)$ is a modified Bessel function of the first kind, $\lambda_{c_1} = \gamma_{c_1}/\alpha_{c_1}$, and $\lambda_{c_2} = \gamma_{c_2}/\alpha_{c_2}$.

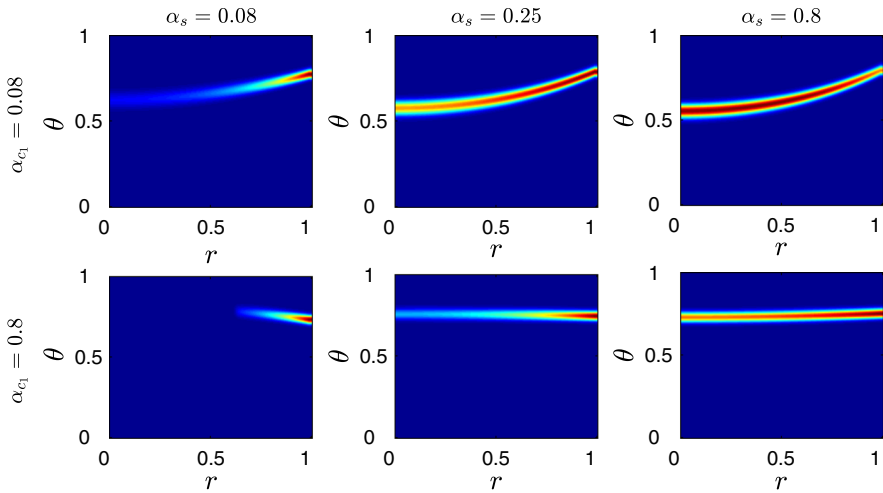


Fig. 6 The surface of cancer cell concentration $n(t, r, \theta)$ at time $t = 100$ for different values of α_s and α_{c_1} without cell diffusion. As the resource becomes more permeable, the cancer cell growth near the center ($r = 0$) is expedited. This increases the overall heterogeneity particularly when the drug permeability is low (first row)

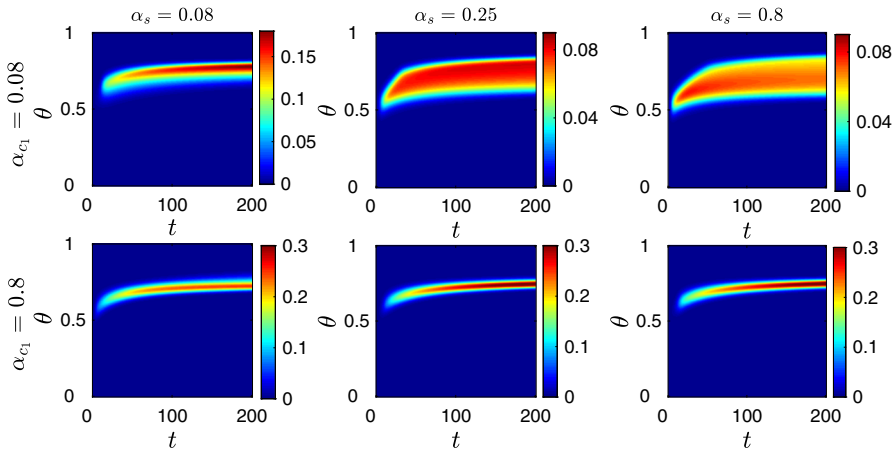


Fig. 7 Phenotype distribution $q(t, \theta)$ on time interval $t \in [0, 200]$ for different values of α_s and α_{c_1} without cell diffusion. The phenotype heterogeneity becomes relatively large when the resource is more permeable compared to the drug (upper-right corner)

and 7. We observe that the cancer cell distribution changes significantly depending on the magnitude of these diffusion coefficients. In Fig. 6, the growth of cancer cells near the center $r = 0$ is accelerated as the permeability of resource increases, while the resistance level of the cell differs depending on the drug permeability. In particular, when the drug permeability is low, the cell population becomes more heterogeneous due to the larger drug dose next to the boundary $r = 1$. Such phenomena are clearly

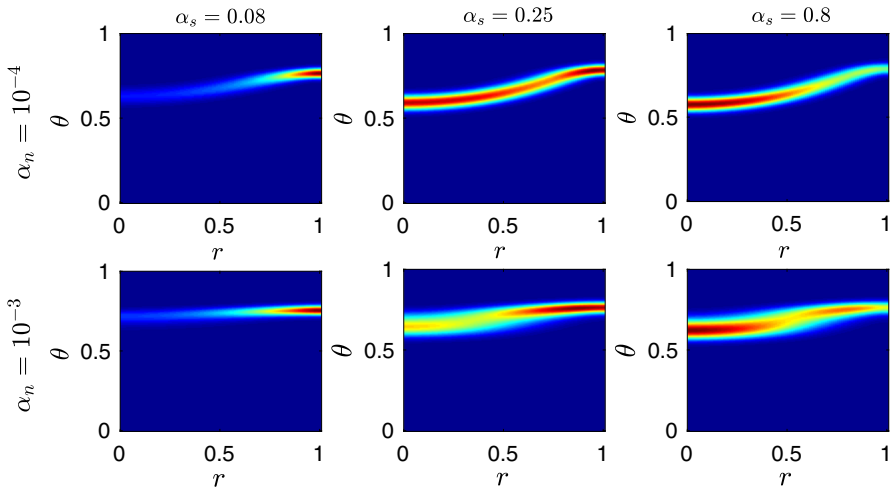


Fig. 8 The surface of cancer cell concentration $n(t = 100, r, \theta)$ with nonzero cell diffusion α_n . The results shown are for different values of α_n and α_s with fixed $\alpha_{c_1} = 0.08$. The cells become homogeneous along r as cell motility, α_n , increases

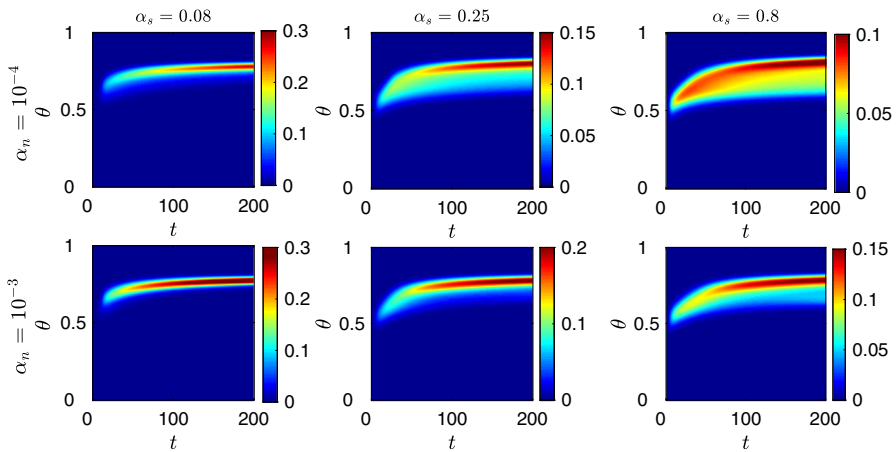


Fig. 9 Phenotype distribution $q(t, \theta)$ on $t \in [0, 200]$ with nonzero cell diffusion α_n . The results are shown for different values of α_n and α_s with fixed $\alpha_{c_1} = 0.08$. As α_n increases, the increased phenotypic homogeneity is reflected in the reduced variance

depicted in Fig. 7, where we observe a larger variance in the phenotype distribution when the cytotoxic drug is less permeable compared to the resource.

Next, we study the effect of cell motility by considering nonzero α_n . In Figs. 8 and 9, we take α_n as 10^{-4} , 10^{-3} , 10^{-2} and test different values of α_s with fixed $\alpha_{c_1} = 0.08$. These are comparable to the first row of Figs. 6 and 7. In contrast to the diffusivity of the resource and the cytotoxic drug, the cell diffusion reduces phenotypic heterogeneity. The cell resistance level becomes more homogeneous in the direction of r as shown in Fig. 8. When $\alpha_n = 10^{-2}$, the cell phenotype density becomes uniform

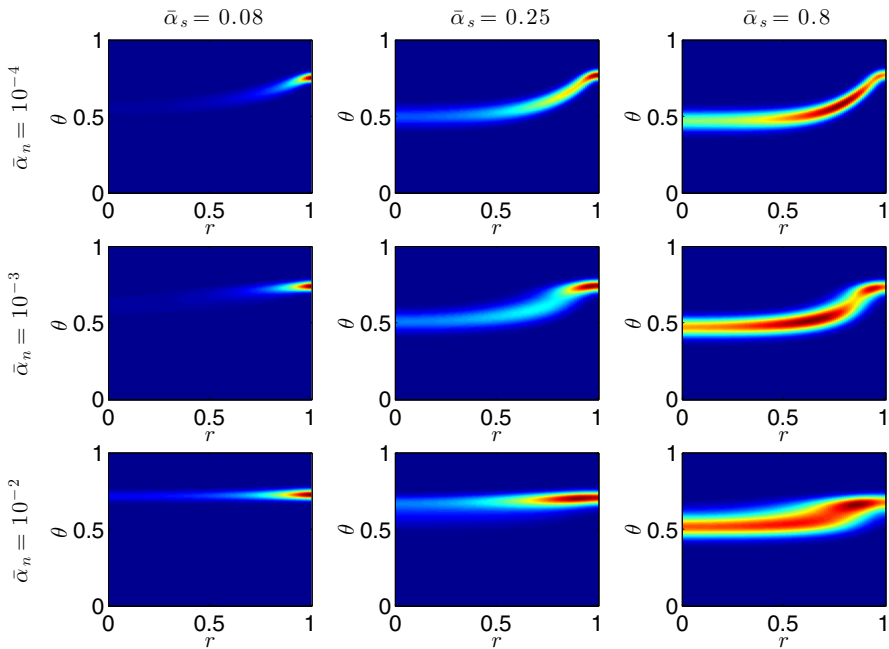


Fig. 10 The surface of cancer cell concentration $n(t = 100, r, \theta)$ with the scaled diffusion, Eq. (17). The cell population becomes more variant compared with the constant coefficient model. Different effects of cell mobility $\bar{\alpha}_n$ and resource permeability $\bar{\alpha}_s$ are observed

in r as in the lower-right corner of Fig. 6. The phenotype distribution $q(t, \theta)$ in Fig. 9 also illustrates that the cells concentrate around a single trait with smaller variance. In addition, we observe an instance of cell clustering yielded by a certain amount of cell mobility, when cells are sufficiently diversified. For instance, in Fig. 8, when $\alpha_n = 10^{-3}$ and α_s is large, the cells near the center and the boundary tend to cluster around different resistance levels, although they eventually merge into a single cluster when $\alpha_n \geq 10^{-2}$.

With our parameter setting, the cancer cell population increases by two orders of magnitude depending on the drug dosage (see Fig. 5), which makes it reasonable to assume that this will affect the cell motility and the permeability of the resources and the drugs. Therefore, we propose to consider the diffusion coefficient as a function of the local cell concentration $\rho(t, r)$. The cell diffusion in Eq. (7) is assumed to be of the following form

$$\alpha_n(\rho) = \frac{\tilde{\alpha}_n}{1 + \bar{\beta}_n \frac{\rho(r,t)}{\rho(r,0)}}, \tag{17}$$

where $\tilde{\alpha}_n = \bar{\alpha}_n(1 + \bar{\beta}_n)$ with $\bar{\alpha}_n$ as the initial magnitude of diffusion coefficient and $\bar{\beta}_n$ being the sensitivity constant to the cell density. The diffusion coefficient decreases with an increased cancer cell population. The coefficient is bounded by zero and the

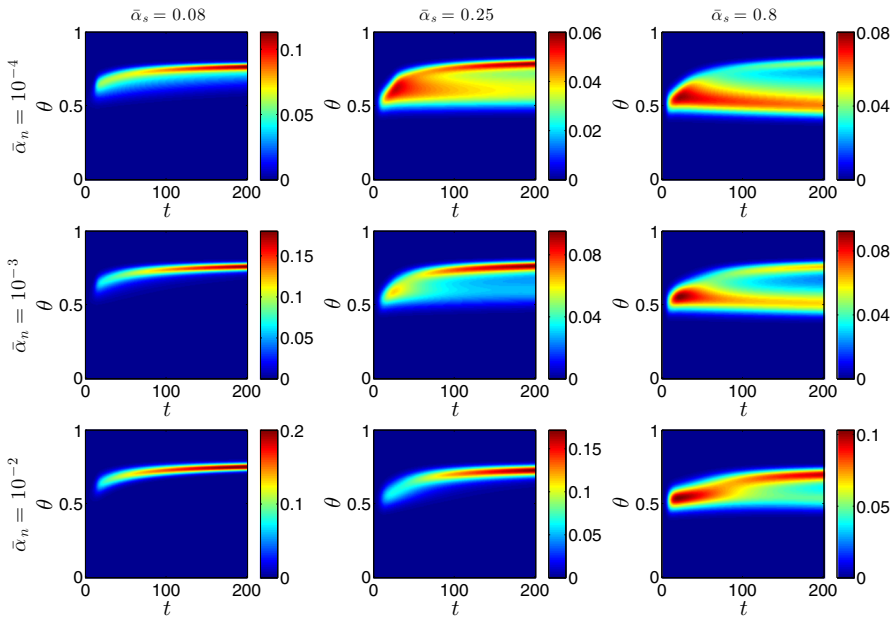


Fig. 11 Phenotype distribution $q(t, \theta)$ on $t \in [0, 200]$ with the scaled diffusion, Eq. (17). The scaled diffusion model provides increased heterogeneity in the resistance level

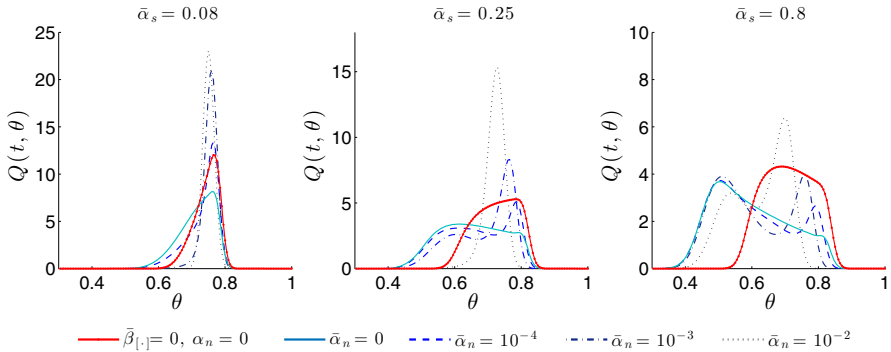


Fig. 12 Phenotype distribution $q(t, \theta)$ at $t = 200$ with and without the scaled diffusion Eq. (17). Compared to the constant diffusion (solid line), the scaled diffusion model depicts a distribution that has a wider spread with respect to the resistance

initial value $\bar{\alpha}_n$, i.e., $0 < \alpha_n(\rho) \leq \bar{\alpha}_n$. The diffusion terms in the other equations are taken similarly as

$$\alpha_s(\rho) = \frac{\bar{\alpha}_s(1 + \bar{\beta}_s)}{1 + \bar{\beta}_s \frac{\rho(r,t)}{\rho(r,0)}}, \quad \alpha_{c_1}(\rho) = \frac{\bar{\alpha}_{c_1}(1 + \bar{\beta}_{c_1})}{1 + \bar{\beta}_{c_1} \frac{\rho(r,t)}{\rho(r,0)}}, \quad \alpha_{c_2}(\rho) = \frac{\bar{\alpha}_{c_2}(1 + \bar{\beta}_{c_2})}{1 + \bar{\beta}_{c_2} \frac{\rho(r,t)}{\rho(r,0)}}.$$

In our simulations, we set the sensitivity constants as $\bar{\beta}_n = \bar{\beta}_s = \bar{\beta}_{c_1} = \bar{\beta}_{c_2} = 0.1$.

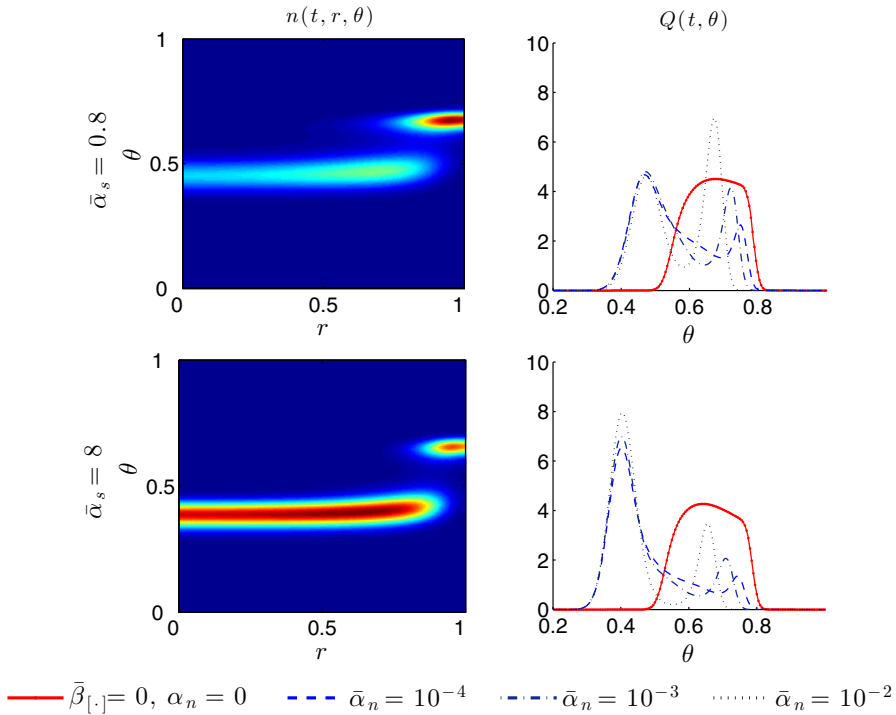


Fig. 13 Cancer cell distribution at $t = 200$ with the scaled diffusion, Eq. (17) and resource $S_1 = 12$. The plots for $n(t, r, \theta)$ correspond to $\bar{\alpha}_n = 10^{-2}$. We observe that with an increased level of resource and cell diffusion, the cell clustering near the center and the boundary become more apparent, and the phenotype distribution becomes a bimodal function

The results showing the effect of scaled diffusion are plotted in Figs. 10 and 11. To compare with the constant diffusion model shown in Figs. 8 and 9, we test different values of $\bar{\alpha}_s$ and $\bar{\alpha}_n$ with fixed $\bar{\alpha}_{c_1} = 0.08$. With the scaled diffusion, the overall heterogeneity in the resistance level increases. In addition, the combined effect of resource permeability $\bar{\alpha}_s$ and cell mobility $\bar{\alpha}_n$, that increases and lessens the cell variation, respectively, can yield multiple clusterings in the cell population. In particular, the phenotype distribution $q(t, \theta)$ plotted in Fig. 11 shows not only the increased variance, but also cells gathering around two different trait values. This is shown more clearly in Fig. 12 where we compare the phenotype distribution $q(t, \theta)$ at $t = 200$ between the constant and the scaled diffusion coefficient model. Furthermore, in Fig. 13, we consider the case where the resource is infused with an increased level of resource as $S_1 = 12$. The separation of the resistance level between the center and the boundary is more apparent, and the corresponding phenotype distribution becomes a bimodal function.

Figures 11, 12, and 13 demonstrate that our model can capture the dynamics that leads to a heterogeneous tumor in space, where different levels of heterogeneity are expressed in different locations in space. It is a one-dimensional caricature of what we

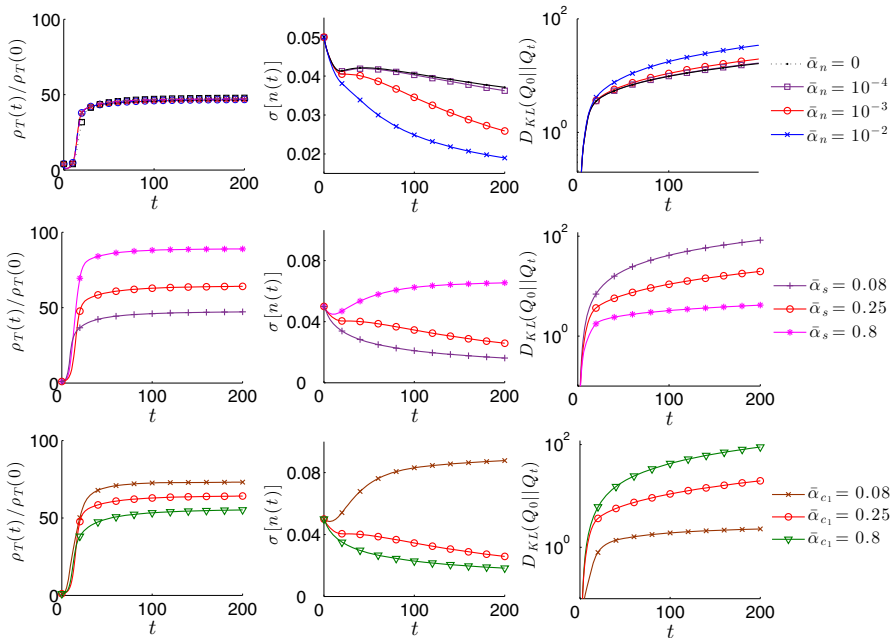


Fig. 14 Effect of diffusion on the cell concentration measured by the relative number of cells $\rho_T(t)/\rho_T(0)$, standard deviation $\sigma[n(t)]$, and the KL divergence $D_{KL}(Q_0||Q_t)$. The other coefficients except the one varied are fixed as $\bar{\alpha}_s = \bar{\alpha}_{c_1} = 0.25, \bar{\alpha}_n = 10^{-3}$

expect to see in 3D tumors *in vivo*. Cells that become drug resistant at certain locations in space may develop into aggregates that have local characteristics of resistance.

We study the quantitative features of the cancer cell population in Fig. 14. The relative total number of cell $\rho_T(t)/\rho_T(0)$, standard deviation of the phenotype distribution $\sigma[n(t)]$, and the deviation from the initial population $D_{KL}(Q_0||Q_t)$ ⁴ are compared for different values of diffusion coefficients. The resource and cytotoxic drug diffusion influences all three measures in opposing directions. While both resource and drug diffusion are critical to the size and the variance of cancer cells, the resource diffusion has slightly more influence on the emerging heterogeneity. However, the deviation from the initial distribution is more affected by the diffusion of the drug.

We also test the combination of an on–off cytotoxic drug and constant cytostatic drug, given by drug schedule 3. This schedule was shown to be effective in eliminating cancer cells (Lorz et al. 2015), which is the reason as of why we study the impact of diffusion on this schedule. Figure 15 shows the total number of cancer cells $\rho_T(t)/\rho_T(0)$ for different values of the diffusion coefficient for the cytotoxic drug,

⁴ $D_{KL}(Q_0||Q_t)$ is the KL divergence from the initial distribution $Q_0(\theta) := Q(t = 0, \theta)$,

$$D_{KL}(Q_0||Q_t) := \int_0^1 Q_0(\theta) \log \frac{Q_0(\theta)}{Q(t, \theta)} d\theta,$$

that represents the divergence of the phenotype distribution from initial time.

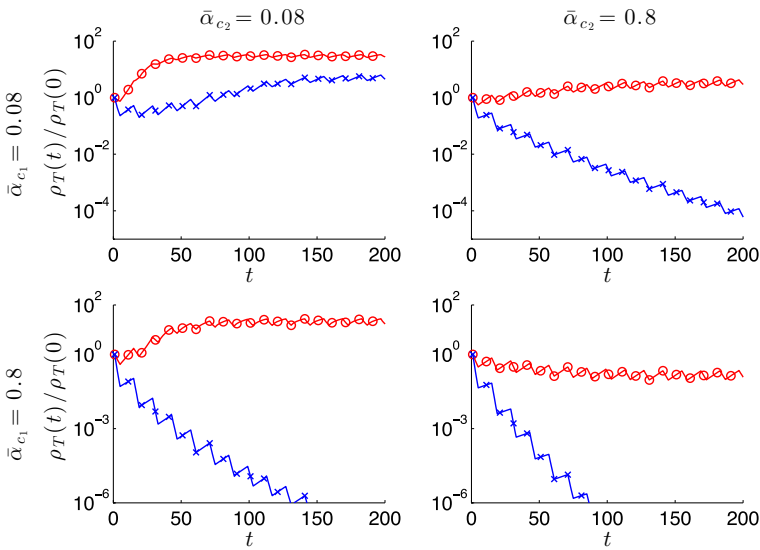


Fig. 15 Total number of cancer cells $\rho_T(t)/\rho_T(0)$ using drug schedule 3 (\circ) and double the dosage of schedule 3 (\times). The resource diffusion and the cell diffusion are fixed as $\bar{\alpha}_s = 0.25$ and $\bar{\alpha}_n = 10^{-3}$, respectively. The cancer cell growth is sensitive to the permeability of the drugs. For the case of $\bar{\alpha}_{c_1} = \bar{\alpha}_{c_2} = 0.08$, doubling the dosage does not prevent the relapse

$\bar{\alpha}_{c_1}$, and the cytostatic drug, $\bar{\alpha}_{c_2}$. The resource diffusion and the cell diffusions are fixed with coefficients $\bar{\alpha}_s = 0.25$ and $\bar{\alpha}_n = 10^{-3}$, respectively, and the cytostatic uptake rate is taken as $\mu_2 = 100$. We see that, as expected, the total number of cells increases when the diffusion of the cytostatic drug is low (as the growth is not effectively inhibited). By doubling the drug dosage to $C_1 = 0.5$ and $C_2 = 1.7$, the drug schedule is more effective in reducing the population of cancer cells except for the case of a low diffusion in both the cytotoxic and cytostatic drugs (upper-left corner) that demonstrates that a relapse is still possible. In particular, the cell concentration surface and the phenotype distribution are plotted in Fig. 16 for the cases when the cells survive ($\bar{\alpha}_{c_1} = \bar{\alpha}_{c_2} = 0.08$) and when they die out ($\bar{\alpha}_{c_1} = \bar{\alpha}_{c_2} = 0.8$). In the former case, the cells that grow are shown to stay close to the center of the initial distribution. Still, this dosage scheme has its advantage as it keeps the level of resistance under control in a moderate range. It also keeps the number of cancer cells relatively smaller than the relapse occurred by the cytotoxic drug.

3.3 Phenotype Selection Depending on Mutation Kernel

Mutation is a key factor that affects the dynamics of resistance in cancer. Here, we aim to model the mutation kernel $M(\theta, \theta')$ in Eq. (7) to explore its impact on the phenotype distribution. The kernel $M(\theta, \theta')$ represents the probability of mutation from a mother cell with phenotype θ' to a daughter cell with phenotype θ . In modeling the mutation kernel, we encode for the asymmetry of mutations in the forward (more

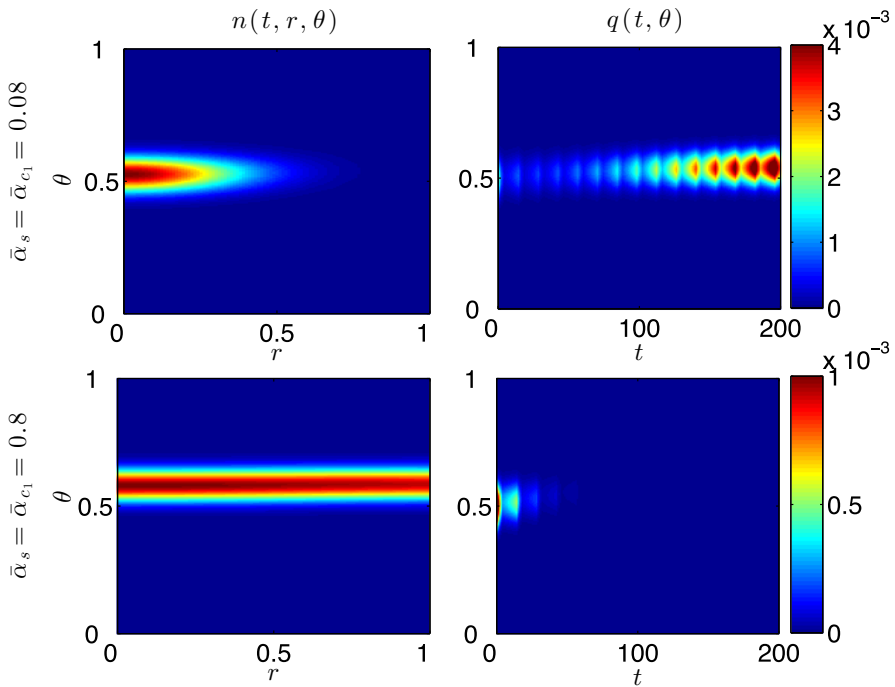


Fig. 16 Cancer cell distribution using drug schedule 3 as in Fig. 15. Cancer cells either die or grow depending on the permeability of the drugs. $n(t = 200, r, \theta)$ shows that the surviving cells are located close to the center of the initial distribution

resistant) and backward (less resistant) directions. In addition, by considering either a smooth function or a discontinuous function for the mutation kernel, we can model mutations either as a continuous process or as a jump process.

We consider the mutation kernel in the following form,

$$M(\theta, \theta') = K(\theta') \exp \left[-\frac{|\theta - \theta'|^2}{\ell(\theta, \theta')^2} \right], \quad \theta, \theta' \in [0, 1], \tag{18}$$

where ℓ is the correlation length that determines the mutation range in the trait space. The correlation length is taken as a function $\ell(\theta, \theta')$ so that the characteristics of mutation can be readily modeled with respect to the resistance level. To model asymmetry, we consider one ℓ in the domain that increases the resistance level, $\ell_u(\theta, \theta')$ on $\theta > \theta'$, and a second ℓ in the complementary domain, $\ell_d(\theta, \theta')$ on $\theta \leq \theta'$. For a regular occurrence of the mutation that depends on the phenotype, we consider ℓ_u as a linear function in terms of $\bar{\theta} := (\theta + \theta')/2$, that is,

$$\ell_u(\theta, \theta') = \ell_u(\bar{\theta}) = (c_{ur} - c_{ul})\bar{\theta} + c_{ul}, \tag{19}$$

where the correlation length changes linearly from c_{ul} at phenotype zero to c_{ur} at phenotype one. Similarly, we denote $\ell_d(\theta, \theta') = (c_{dr} - c_{dl})\bar{\theta} + c_{dl}$. The irreversibility

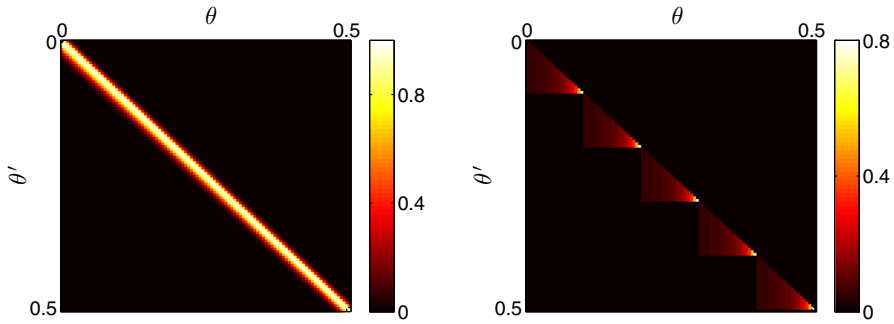


Fig. 17 A mutation kernel, $M(\theta, \theta')$, that is based on a Gaussian function with linear correlation length (left) and a piecewise linear function (right). The kernels are zoomed on $\theta, \theta' \in [0, 0.5]$

of the mutation can be imposed by $\ell_d = 0$ and less strictly by taking smaller correlation lengths when $\theta \leq \theta'$ compared to $\theta > \theta'$, i.e., $c_{ur} \geq c_{dr}$ and $c_{ul} \geq c_{dl}$. In our simulations, we choose $c_{ul} = 0.02$, $c_{ur} = 0.01$, $c_{dl} = 10^{-10}$, and $c_{dr} = 0.01$ (see Fig. 17). The mutation in the upper direction is reduced by considering a negative slope for ℓ_u , and to avoid saturation at the highest resistance level, we allow backward mutation near $\theta = 1$.

Although a Gaussian kernel with a smooth correlation function can model the mutations that occur regularly, we consider a second mutation kernel that reduces the probability of mutation occurring at certain trait values. This can be obtained, e.g., by considering a mutation kernel based on piecewise linear functions defined on n_D partitions,

$$M(\theta, \theta') = \begin{cases} \sum_{i=1}^{n_D} K(\theta')(\theta - \theta_{i-1}) \chi_{\Omega_i \times \Omega_i}^{(\theta, \theta')}, & \theta \geq \theta', \\ 0, & \text{otherwise,} \end{cases} \tag{20}$$

where $\{\Omega_i\}_{i=1}^{n_D}$ is a partition of $[0, 1]$ with boundaries denoted as $\Omega_i = [\theta_{i-1}, \theta_i]$, and χ_A is an indicator function on A . The boundary values of Ω_i correspond to phenotype values that may be more difficult to mutate away from⁵. Figure 17 shows an example of a mutation kernel using this form of correlation function. We take $n_D = 10$ uniform partition of $[0, 1]$. We emphasize that these are arbitrary choices.

To study the impact of these mutation kernels, we test for the case when the diffusion constants are $\bar{\alpha}_n = 10^{-3}$, $\bar{\alpha}_s = 0.8$, 0.08 , and $\bar{\alpha}_{c_1} = 0.08$ using drug schedule 1. We fix $w = 0.1$ and compare the result with the reference phenotype distribution without mutation, $w = 0$. Figures 18 and 19 show the phenotype distribution $q(t, \theta)$ corresponding to the two mutation kernels shown in Fig. 17, using the Gaussian kernel (18) and piecewise linear (20) functions. In Fig. 18, we observe that smooth linear correlation lengths increase the variance in $q(t, \theta)$ and regularize the distribution. In spite of the diffusion terms, our model still has a tendency to concentrate near

⁵ Similar behavior can be modeled using the Gaussian kernel (18) by considering a piecewise continuous correlation length on $\{\Omega_i\}$. For instance, $\ell_u(\theta, \theta') = \ell_i(\bar{\theta})$ on each $\bar{\theta} \in \Omega_i$, where $\ell_i(\bar{\theta})$ is a quadratic function that decays as $\bar{\theta}$ approaches the partition boundary.

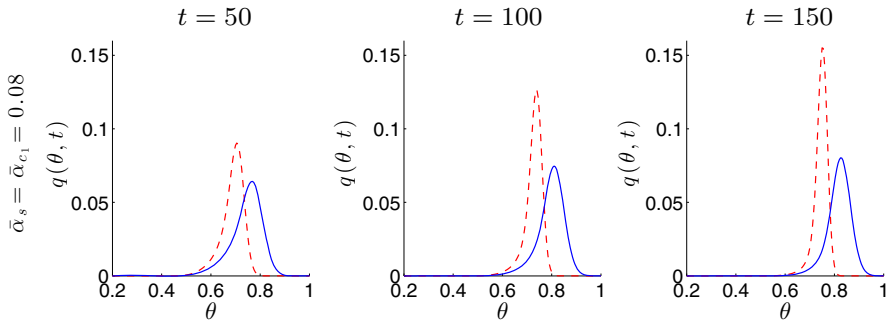


Fig. 18 Comparison of the phenotype distribution $q(t, \theta)$ without mutation (dashed line) and with mutation (solid line) using a Gaussian mutation kernel (18) and $w = 0.1$. This mutation expedites the occurrence of resistant cells, while preventing an extreme localization at a single trait

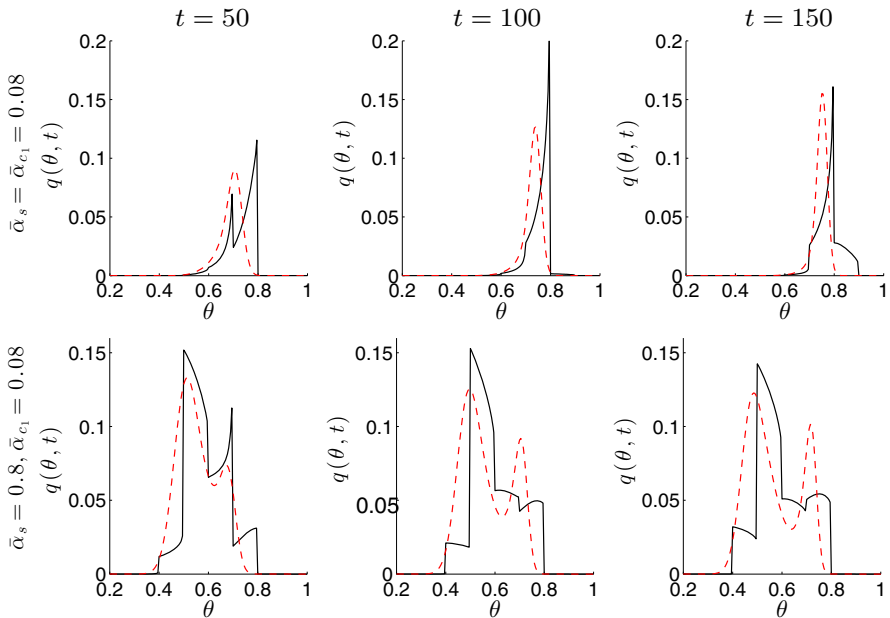


Fig. 19 Comparison of the phenotype distribution $q(t, \theta)$ without mutation (dashed line) and with mutation (solid line) using a piecewise linear mutation kernel (20) and $w = 0.1$. This mutation kernel allows for less frequent mutations in certain trait values

the point where the maximum growth rate is achieved. This type of mutation kernel prevents the phenotype distributions from being well localized after long-time simulations (Greene et al. 2014). In addition, the phenotype distribution is smoothly shifted toward the higher resistance levels due to the asymmetry in the kernel. The quantitative effect of mutation comparable to Fig. 14 is shown in Fig. 20. The correlation length of the mutation increases all three features including the mean $E[n(t)]$ and standard

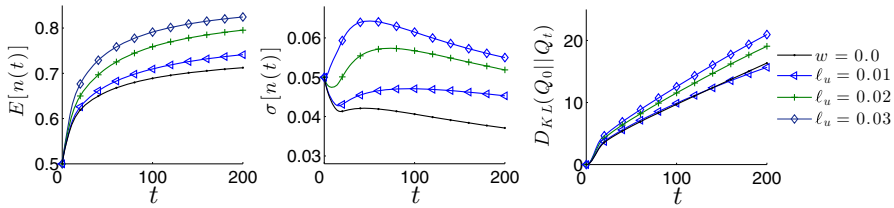


Fig. 20 Effect of mutation on the cell concentration measured by the mean $E[n(t)]$ and standard deviation of the phenotype $\sigma[n(t)]$, and the KL divergence $D_{KL}(Q_0||Q_t)$

deviation $\sigma[n(t)]$ of the resistance level, and the deviation from the initial distribution $D_{KL}(Q_0||Q_t)$.

In contrast to the linear case, the phenotype distribution using a piecewise linear mutation kernel shows distinctive features. In Fig. 19, we observe that cancer cells accumulate before crossing the bottleneck trait values. This makes the phenotype distribution different from the reference distribution that is rather close to a symmetric unimodal function. In the case of $\alpha_s = \alpha_{c_1} = 0.08$ at time $t = 100$, an even higher peak shows next to $\theta = 0.8$, yet, a small number of cells begin to cross the blockage point at $t = 150$.

In most studies, modeling mutations using integral transformations results with an increased variance due to the smoothing of the cell distribution. Our approach provides possible alternative sources for obtaining irregularity in the cell distribution.

4 Conclusion

In this paper, we developed a mathematical model that describes the evolution of drug resistance in cancer cells with regard to the spatial dynamics of the resource and drugs, cell motility, and phenotypic mutation. In contrast to the original Lorz model, our model allows the emergence of partial resistance levels. We emphasize that this modification is shown to result with tumor dynamics that is more relevant to the biology. Moreover, by assuming a drug response that depends on the concentration, we encode for the sensitivity of the resistance level to high drug dosages, that is consistent with the observations made in Mumenthaler et al. (2015) and Garvey et al. (2016). We show that increased drug concentrations are correlated with a delayed relapse, though with higher resistant traits being selected. We further show that an on-off therapy schedule also selects for more resistant traits when compared with a continuous schedule of identical total drug concentrations.

Our model incorporates cell diffusion and mutation into the resistance dynamics. While the resource permeability increases the phenotypic heterogeneity by allowing various level of cells to grow in distinct locations, increased level of diffusion in the cell motility and the drug permeability play an opposite role. Since the cell population is highly sensitive to the diffusion, we emphasize that it is important to consider diffusion coefficients that depend on the local cell concentrations. The combined effect of the diffusion terms in our model yields distinctive cell populations. We also show that under certain conditions, our model predicts the emergence of a heterogeneous tumor

in which cancer cells of different resistance levels coexist in different areas in space. Finally, the mutation term, parametrized by the range of mutation allowed in each resistance level, increases the phenotypic variation.

Although the assumption of radial symmetry is consistent with experimental evidence on tumor spheroids of small size (Yu et al. 2004), it is no longer valid for larger, vascularized tumors (Anderson et al. 2006; Trédan et al. 2007). We intend to extend our model to a full 2D system. This will allow us to investigate the spatial dependency of intra-tumor heterogeneity in a more general setting. In addition, we propose to extend our theoretical results by combining them with more recent analytical results of phenotypic structured selection models (Mirrahimi and Perthame 2015; Jabin and Schram 2016). Another drawback of our model is that the trait variable represents the resistance level regarding the cytotoxic drug without considering the cytostatic drug. We aim to study multi-drug resistance (Panagiotopoulou et al. 2010) by considering a multi-dimensional trait variable subject to different classes of drugs and other phenotypes. It will be of great interest to extend the present model to specific clinical problems. Although mapping the heterogeneity in the physical and phenotypic space in vivo is not possible with current technology, we look forward to validating and quantifying our model observations, and exploring various optimal chemotherapy scheduling (Schättler and Ledzewicz 2015) while incorporating the heterogeneity of the drug response.

Acknowledgements The work of DL was supported in part by the National Science Foundation under Grant Number DMS-1713109, by the John Simon Guggenheim Memorial Foundation, by the Simons Foundation, and by the Jayne Koskinas and Ted Giovanis Foundation.

References

- Amir ED, Davis KL, Tadmor MD, Simonds EF, Jacob Levlne H, Bendall SC, Shenfeld DK, Krishnaswamy S, Nolan GP, Pe'er D (2013) viSNE enables visualization of high dimensional single-cell data and reveals phenotypic heterogeneity of leukemia. *Nat Biotechnol* 31(6):545–552
- Anderson AR, Chaplain M (1998) Continuous and discrete mathematical models of tumor-induced angiogenesis. *Bull Math Biol* 60(5):857–899
- Anderson AR, Weaver AM, Cummings PT, Quaranta V (2006) Tumor morphology and phenotypic evolution driven by selective pressure from the microenvironment. *Cell* 127(5):905–915
- Ariffin AB, Forde PF, Jahangeer S, Soden DM, Hinchion J (2014) Releasing pressure in tumors: What do we know so far and where do we go from here? *Cancer Res* 74:2655–62
- Birkhead BG, Rakin EM, Gallivan S, Dones L, Rubens RD (1987) A mathematical model of the development of drug resistance to cancer chemotherapy. *Eur J Cancer Clin Oncol* 23:1421–1427
- Brodie EDIII (1992) Correlational selection for color pattern and antipredator behavior in the garter snake *Thamnophis ordinoides*. *Evolution* 46:1284–1298
- Corbett T, Griswold D, Roberts B, Peckham J, Schabel F (1975) Tumor induction relationships in development of transplantable cancers of the colon in mice for chemotherapy assays, with a note on carcinogen structure. *Cancer Res* 35:2434–2439
- de Bruin EC, Taylor TB, Swanton C (2013) Intra-tumor heterogeneity: lessons from microbial evolution and clinical implications. *Genome Med* 5:1–11
- de Pillis LG, Raduskaya AE, Wiseman CL (2005) A validated mathematical model of cell-mediated immune response to tumor growth. *Cancer Res* 65:7950–7958
- de Pillis LG, Savage H, Raduskaya AE (2014) Mathematical model of colorectal cancer with monoclonal antibody treatments. *Br J Med Med Res* 4:3101–3131
- Fodal V, Pierobon M, Liotta L, Petricoin E (2011) Mechanisms of cell adaptation: When and how do cancer cells develop chemoresistance? *Cancer J* 17(2):89–95

- Foo J, Michor F (2014) Evolution of acquired resistance to anti-cancer therapy. *J Theor Biol* 355:10–20
- Garvey CM, Spiller E, Lindsay D, Ct Chiang, Choi NC, Agus DB, Mallick P, Foo J, Mumenthaler SM (2016) A high-content image-based method for quantitatively studying context-dependent cell population dynamics. *Sci Rep* 6(29752):1–12
- Gerlinger M, Rowan AJ, Horswell S, Larkin J, Endesfelder D, Gronroos E, Martinez P (2012) Intratumor heterogeneity and branched evolution revealed by multiregion sequencing. *N Engl J Med* 366:883–892
- Gillet JP, Gottesman MM (2010) Mechanisms of multidrug resistance in cancer. *Methods Mol Biol* 596:47–76
- Goldie JH, Coldman AJ (1979) A mathematical model for relating the drug sensitivity of tumors to their spontaneous mutation rate. *Cancer Treat Rep* 63:1727–1733
- Goldie JH, Coldman AJ (1983a) A model for resistance of tumor cells to cancer chemotherapeutic agents. *Math Biosci* 65:291–307
- Goldie JH, Coldman AJ (1983b) Quantitative model for multiple levels of drug resistance in clinical tumors. *Cancer Treat Rep* 67:923–931
- Gottesman MM (2002) Mechanisms of cancer drug resistance. *Annu Rev Med* 53:615–627
- Gottesman MM, Fojo T, Bates SE (2002) Multidrug resistance in cancer: role of ATP-dependent transporters. *Nat Rev Cancer* 2(1):48–58
- Greene J, Lavi O, Gottesman MM, Levy D (2014) The impact of cell density and mutations in a model of multidrug resistance in solid tumors. *Bull Math Biol* 74:627–653
- Grothey A (2006) Defining the role of panitumumab in colorectal cancer. *Community Oncol* 3:6–10
- Hanahan D, Weinberg RA (2011) Hallmarks of cancer: the next generation. *Cell* 144(5):646–674
- Iwasa Y, Nowak MA, Michor F (2006) Evolution of resistance during clonal expansion. *Genetics* 172:2557–2566
- Jabin PE, Schram RS (2016) Selection-mutation dynamics with spatial dependence pp 1–21
- Kimmel M, Swierniak A, Polanski A (1998) Infinite-dimensional model of evolution of drug resistance of cancer cells. *J Math Syst Estim Control* 8:1–16
- Komarova N (2006) Stochastic modeling of drug resistance in cancer. *Theor Popul Biol* 239(3):351–366
- Lavi O, Gottesman MM, Levy D (2012) The dynamics of drug resistance: a mathematical perspective. *Drug Resist Update* 15(1–2):90–97
- Lavi O, Greene J, Levy D, Gottesman MM (2013) The role of cell density and intratumoral heterogeneity in multidrug resistance. *Cancer Res* 73:7168–7175
- Lavi O, Greene J, Levy D, Gottesman MM (2014) Simplifying the complexity of resistance heterogeneity in metastatic cancer. *Trend Mol Med* 20:129–136
- Lorz A, Lorenzi T, Hochberg ME, Clairambault J, Perthame B (2013) Populational adaptive evolution, chemotherapeutic resistance and multiple anti-cancer therapies. *ESAIM Math Model Numer Anal* 47:377–399
- Lorz A, Lorenzi T, Clairambault J, Escargueil A, Perthame B (2015) Modeling the effects of space structure and combination therapies on phenotypic heterogeneity and drug resistance in solid tumors. *Bull Math Biol* 77:1–22
- Medema JP (2013) Cancer stem cells: the challenges ahead. *Nat Cell Biol* 15(4):338–344
- Michor F, Nowak MA, Iwasa Y (2006) Evolution of resistance to cancer therapy. *Curr Pharm Des* 12:261–271
- Minchinton AI, Tannock IF (2006) Drug penetration in solid tumours. *Nat Rev Cancer* 6:583–592
- Mirrahimi S, Perthame B (2015) Asymptotic analysis of a selection model with space. *J Math Pures Appl* 104:1108–1118
- Mumenthaler SM, Foo J, Choi NC, Heise N, Leder K, Agus DB, Pao W, Michor F, Mallick P (2015) The impact of microenvironmental heterogeneity on the evolution of drug resistance in cancer cells. *Cancer Inform* 14:19–31
- Panagiotopoulou V, Richardson G, Jensen OE, Rauch C (2010) On a biophysical and mathematical model of Pgp-mediated multidrug resistance: understanding the space-time dimension of MDR. *Eur Biophys J* 39:201–211
- Panetta JC (1998) A mathematical model of drug resistance: heterogeneous tumors. *Math Biosci* 147:41–61
- Rainey PB, Travisano M (1998) Adaptive radiation in a heterogeneous environment. *Nature* 2:69–72
- Roose T, Chapman SJ, Maini PK (2007) Mathematical models of avascular tumor growth. *SIAM Rev* 49(2):179–208
- Schättler H, Ledzewicz U (2015) Optimal control for mathematical models of cancer therapies, 1st edn. Springer, Berlin

- Simon R, Norton L (2006) The norton-simon hypothesis: designing more effective and less toxic chemotherapeutic regimens. *Nat Clin Pract Oncol* 3:406–407
- Swierniak A, Kimmel M, Smieja J (2009) Mathematical modeling as a tool for planning anticancer therapy. *Eur J Pharmacol* 625(1–3):108–121
- Teicher BA (2006) *Cancer drug resistance*. Humana Press, Totowa
- Tomasetti C, Levy D (2010) An elementary approach to modeling drug resistance in cancer. *Math Biosci Eng* 7:905–918
- Trédan O, Galmarini CM, Patel K, Tannock IF (2007) Drug resistance and the solid tumor microenvironment. *J Natl Cancer Inst* 99:1441–1454
- Vaupel P, Kallinowski F, Okunieff P (1989) Blood flow, oxygen and nutrient supply, and metabolic microenvironment of human tumors: a review. *Cancer Res* 49:6449–6465
- Wosikowski K, Silverman JA, Bishop P, Mendelsohn J, Bates SE (2000) Reduced growth rate accompanied by aberrant epidermal growth factor signaling in drug resistant human breast cancer cells. *Biochimica et Biophysica Acta* 1497(2):215–226
- Wu A, Louterback K, Lambert G, Estévez-Salmerón L, Tlsty TD, Austin RH, Sturm JC (2013) Cell motility and drug gradients in the emergence of resistance to chemotherapy. *Proc Natl Acad Sci* 110(40):16,103–16,108
- Yu P, Mustata M, Peng L, Turek JJ, Melloch MR, French PM, Nolte DD (2004) Holographic optical coherence imaging of rat osteogenic sarcoma tumor spheroids. *Appl Opt* 43:4862–4873